The star-formation history of the Universe from the stellar populations of nearby galaxies

Alan Heavens[1], Benjamin Panter[1], Raul Jimenez[2] & James Dunlop[1]

[1]*Institute for Astronomy, University of Edinburgh, Blackford Hill, Edinburgh EH9 3HJ, UK*
[2]*Department of Physics and Astronomy, University of Pennsylvania, 209 South 33rd Street, Philadelphia, Pennsylvania 19104-6396, USA*

The determination of the star-formation history of the Universe is a key goal of modern cosmology, as it is crucial to our understanding of how galactic structures form and evolve. Observations[1–12] of young stars in distant galaxies at different times in the past have indicated that the stellar birthrate peaked some eight billion years ago before declining by a factor of around ten to its present value. Here we report an analysis of the 'fossil record' of the current stellar populations of 96,545 nearby galaxies, from which we obtained a complete star-formation history. Our results broadly support those derived from high-redshift galaxies. We find, however, that the peak of star formation was more recent—around five billion years ago. We also show that the bigger the stellar mass of the galaxy, the earlier the stars were formed, which indicates that high- and low-mass galaxies have very different histories.

The optical stellar spectrum of a galaxy can be used as a probe of both its past star-formation history, and the metallicity of its gas as a function of time. The spectra of a large sample of nearby galaxies therefore acts as a useful fossil record of the star-formation rate of the Universe, allowing estimates of the star-formation rate over a very wide range of cosmic time, from the same internally consistent data set, and with very small statistical errors. The alternative is to use the finite speed of light to view galaxies at different cosmic epochs, and to look for signs of recent star formation. The present method decouples the star formation from the mass assembly—it takes into account all stars which end up in normal galaxies today, and it is much less sensitive to the large corrections, for extinction and for unobserved small galaxies, which must be applied to high-redshift studies.

The spectral data used in this analysis come from the Sloan Digital Sky Survey data release 1 (SDSS DR1), from an area of 1,360 square degrees. The main sample has red apparent magnitude limits of $15.0 \leq m_R \leq 17.77$, and we also place a limit on surface brightness of $\mu_R < 23.0$ (see ref. 13 for discussion of this). The redshift range is $0.005 < z < 0.34$, with a median of 0.1. This leaves 96,545 galaxies in this study. Full details of the SDSS are available at http://www.sdss.org/. The spectra are top-hat smoothed to 20-Å resolution, for comparison with the models of ref. 14, and emission-line regions are removed, as these are generally non-stellar and outside the scope of the theoretical model employed.

The speed of MOPED (see below) means we are not restricted to assuming simple parametrizations of the star-formation history[15,16]. For each spectrum, we recover the mass of stars created in 11 time periods, which are mostly equally spaced logarithmically in look-back time, separated by factors of 2.07, but with the first boundary at a redshift of two. We assume a Salpeter initial mass function, and a cosmology given by the best-fitting parameters determined by the WMAP satellite[17]: $\Omega_m = 0.27$, $\Omega_v = 0.73$, $H_0 = 71\,\mathrm{km\,s^{-1}\,Mpc^{-1}}$. For each time period, we also recover the average metallicity of the gas, and an overall dust parameter for the galaxy, assuming a Large Magellanic Cloud extinction curve[18]. Thus we have a 23-dimensional parameter space to search. A straightforward maximum-likelihood solution using the full spectrum of all the SDSS galaxies is impractical, so we use the patented radical lossless data compression algorithm MOPED[19] to compress each spectrum to 23 numbers, and we find the set of 23 parameters which fit these MOPED coefficients most accurately. The massive data compression allows much faster determination of the parameters and the errors on them, and, importantly, can be shown to be lossless in ideal cases, in the sense that the error bars are not increased by using the MOPED coefficients rather than the entire spectrum. More details are given in papers developing and testing MOPED[19–21].

With this method, we obtain the mass of stars created in each galaxy g in each period of time (relative to the time of emission of the galaxy light), $\delta M_{\star g}(t)$. After redistribution of the stars to a set of time bins fixed in cosmic time, we estimate the star-formation rate per unit co-moving volume by $\dot{\rho}_\star(t) = \sum_g \delta M_{\star g}/(V_{\max}\delta t)$, where δt is the width of the time bin. $V_{\max}$ is the maximum volume in which the galaxy could be placed and still contribute to the star-formation rate estimate at time t. We have no knowledge of the star-formation rate at redshifts less than the observed redshift of the galaxy, so this introduces a redshift cutoff. Other limits come from the magnitude and surface brightness limits of the sample. These are calculated by computing the galaxy spectrum as a function of time (from the recovered star-formation-rate parameters) and computing the expected observed R-band flux and surface brightness. We take account of the three-arcsec fibre aperture by correcting the spectrum upwards by the ratio of the flux in R in a petrosian radius (determined by the photometry) to the fibre flux. For individual

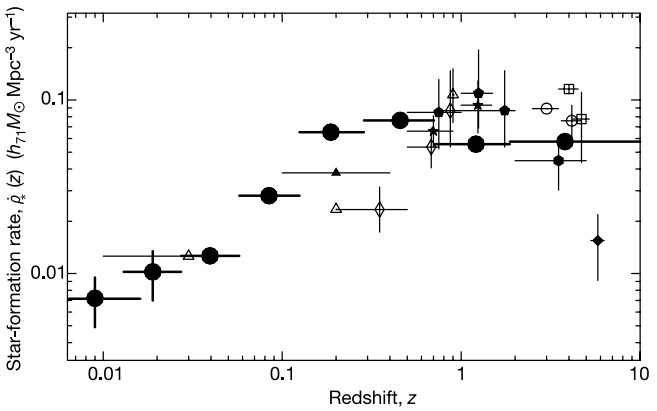

Figure 1 The star-formation history of the Universe. The star-formation rate recovered from the 'fossil record' in the SDSS is shown by the eight large filled circles. The horizontal error bars represent the size of the bin in redshift. Vertical error bars represent bootstrap errors, and are invisibly small for most bins. Also shown are independent determinations using instantaneous measurements of the star-formation rate, as follows: Hα measurements (open triangles) at $z \simeq 0.03$ (ref. 1), $z \simeq 0.2$ (ref. 5) and $z \simeq 0.9$ (ref. 6); ultraviolet from Subaru[11] (open squares), GOODS[12] (filled diamond), HST and so on[3] (open circles), CFRS[2] (open diamonds), HDF[4] (filled pentagons), galaxies[7] (star shapes) and galaxies[8] (filled triangle). The filled hexagon at $z = 3.5$ represents a new estimate of the star-formation density provided by the sub-mm galaxies in the redshift range $2 < z < 5$. This was derived by integrating the sub-mm source number counts[9] down to $S_{850\,\mu m} = 1$ mJy, and assuming that 75% of such sources lie at $z > 2$ (in line with recent redshift measurements[10]). In general, the agreement is very good. However, there are two important results in our study which result from the extremely small vertical error bars. First, we find that 26% of the mass of stars in the present-day Universe were formed at $z > 2$. Second, while we confirm the previous measurements of a generally high level of star-formation activity at $z \simeq 1$, we find that global star-formation density peaked at significantly lower redshifts than previously claimed, in the bin spanning the redshift range $0.3 < z < 0.8$. The reason for this difference is clarified in Fig. 2. h_{71} is the Hubble constant in units of $71\,\mathrm{km\,s^{-1}\,Mpc^{-1}}$.

galaxies this is likely to fail, but for the population as a whole there is evidence from the colours[16] that fibre-placing is such that there is no significant systematic difference in the sampling of stellar populations by the spectroscopy and photometry.

In Fig. 1 we show the co-moving star-formation rate determined by MOPED and SDSS DR1, as a function of redshift, along with results from other determinations, largely based on instantaneous star-formation rate indicators (ultraviolet flux, Hα emission, sub-millimetre (mm) emission and so on). At a basic level, the new data show good agreement over the redshift range of $0.01 < z < 6$. The low-redshift decline of the star-formation rate is clearly seen, and the rate also appears to have flattened. Moreover, the level of star-formation activity inferred at high redshift ($z > 2$) is in rather good agreement with the completely independent values inferred from observations of high-redshift galaxies, suggesting that the dust corrections made in such studies are reasonable, if a little over-estimated. The broad agreement of the star-formation rate determined locally from the fossil record of the SDSS with the determinations from high-redshift galaxies gives support for the copernican principle: that is, that the Earth has no special location in the Universe. It also supports the current standard cosmological model, as the volume elements assumed in the high-redshift studies are sensitive to the cosmological parameters. Note, however, that this does assume that our assumption about the initial mass function is reasonable, as we are inferring the number of early-forming high-mass stars (now dead) from the numbers of early-forming low-mass stars, which are still contributing to the galaxy spectrum.

One of our main results is that the period of star formation is broader than previously thought, and occurs at a lower redshift $z \simeq 0.6$, rather than one or more. Specifically, we find that 26% of the mass of stars in the present-day Universe was formed at $z > 2$ (compare ref. 22). The average metallicity rises from 0.44 (relative to the solar value) at high z to a peak of 0.8 at $z \simeq 1$ before declining to a level around 0.25 at the present time.

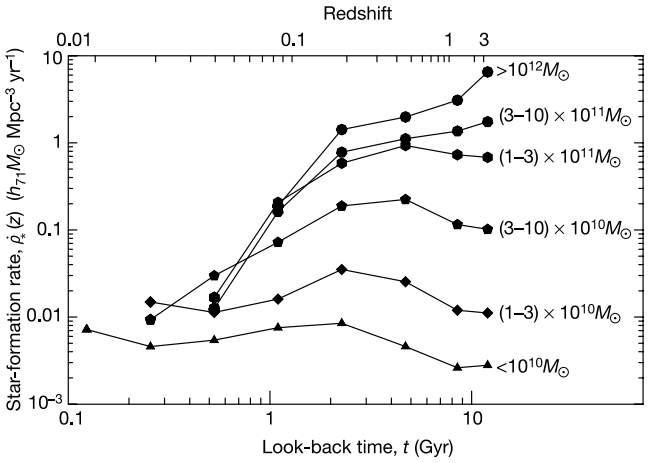

Figure 2 The star-formation rate as a function of the observed stellar mass of the galaxy. For clarity, the curves are offset vertically, successively by 0.5 log units, except for the most massive galaxies, which are offset by an additional 1.0. Note the clear trend for galaxies with larger present-day stellar mass to have formed their stars earlier. The bulk of the star-formation rate at $z \simeq 0.5$ comes from galaxies with present-day stellar masses in the range $3 - 30 \times 10^{10} M_\odot$. Note that the graph makes no statement about when the masses were aggregated. To test further the robustness of our findings we have reconstructed the star-formation history, changing the dust model and the theoretical stellar population models. The shape of the star-formation history is hardly changed by changing the dust model to the Calzetti extinction law[28], or by using Bruzual–Charlot[29] stellar population models; the latter allows us to assess the effect of systematic errors in our determination of the star-formation rate, because the Jimenez and Bruzual–Charlot models are based on different stellar interior and atmosphere models.

As we explain below, we believe our result differs because it includes the contributions made by all galaxies over a very wide mass range, extending down to galaxies with $L \approx 2 \times 10^{-3} L_\star$, where $L_\star$ is the characteristic luminosity of a large galaxy. Note that virtually all 96,545 galaxies contribute to the $z > 0.3$ bins, so the statistical errors (bootstrap estimates) are negligible in comparison with modelling uncertainties and residual uncertainties in flux calibration. We also note that because we are not dominated by statistical errors, the errors are smaller in this approach than by analysing, for example, some appropriately-weighted average of the spectra themselves. Supplementary Fig. 1 shows that parameter recovery is robust.

Our second major result is apparent when we present the star-formation history of the sample, divided into different ranges of observed stellar mass. We see clearly in Fig. 2 that the redshift at which star-formation activity peaks is an essentially monotonically increasing function of final stellar mass. Star-formation activity in the galaxies in the lowest-mass bins ($M_\star \simeq 10^{10} M_\odot$, where $M_\star$ is the stellar mass and $M_\odot$ the solar mass) peaked at $z \simeq 0.2$, whereas for galaxies that are an order of magnitude more massive the peak lies at $z \simeq 0.5$. At still higher masses, galaxies with masses comparable to a present-day $L_\star$ galaxy appear to have experienced a peak in activity at $z \simeq 0.8$, whereas the highest-mass systems ($M_\star > 10^{12} M_\odot$) show a monotonic decline in star-formation rate in our data, with any peak constrained to lie at $z > 2$. This provides a natural explanation for why the most massive star-forming systems, such as the selected luminous, sub-mm galaxies, should largely be found to lie at high redshifts ($z > 2$; ref. 10), while at the same time providing further evidence that the bright sub-mm galaxies are indeed the progenitors of today's massive ellipticals[23]. The importance of low-mass systems in low-redshift star formation has been noted (see, for example, refs 24 and 25).

Indeed, the strong mass-dependence of the star-formation history also provides a natural explanation of the high redshift of peak star-formation activity seen in other surveys, because they are sensitive only to the most massive objects. That we have now discovered that global star-formation activity in fact peaks at rather a modest redshift is because the peak epoch of star-formation activity in objects of lower (present-day stellar) masses ($< 3 \times 10^{11} M_\odot$) was at $z \lesssim 0.5$, and because such lower-mass galaxies make a significant contribution to the overall star-formation density. Given present-day observational capabilities, this result could only be revealed by a method such as used here, because the fossil record approach allows us to explore the star-formation history of galaxies spanning over two decades in mass. Supplementary Fig. 2 demonstrates consistent results from volume-limited subsamples.

Finally, we note that the mass dependence of peak star-formation epoch revealed in Fig. 2 appears to mirror the mass dependence of black-hole activity as recently seen in redshift surveys of both radio-selected[26] and X-ray-selected[27] active galactic nuclei. Such apparently anti-hierarchical behaviour ('downsizing') is in fact quite consistent with the standard cosmological model, in which galaxies form in small units and merge—our method makes no statement about whether the stellar mass at high redshift was in smaller units or not. The behaviour we see is based on the present-day stellar mass of the galaxies, and in general we would expect more massive systems to be part of large-scale overdensities, in which first star formation would occur earlier. Furthermore, these results suggest a very different formation history for low- and high-mass systems, because the mass assembly proceeds in the opposite direction to the star formation. (This will be explored in a separate paper.) □

Received 19 December 2003; accepted 9 March 2004; doi:10.1038/nature02474.

1. Gallego, J., Zamorano, J., Aragon-Salamanca, A. & Rego, M. The current star formation rate of the local Universe. *Astrophys. J. Lett.* **455,** 1–4 (1995).
2. Lilly, S. J., Le Fevre, O., Hammer, F. & Crampton, D. The Canada-France redshift survey: The luminosity density and star formation history of the Universe to $z \sim 1$. *Astrophys. J. Lett.* **460,** 1–4 (1996).
3. Steidel, C. C., Giavalisco, M., Pettini, M., Dickinson, M. & Adelberger, K. L. Spectroscopic confirmation of a population of normal star-forming galaxies at redshifts $z > 3$. *Astrophys. J. Lett.* **462,** 17–21 (1996).
4. Connolly, A. J., Szalay, A. S., Dickinson, M., Subbarao, M. U. & Brunner, R. J. The evolution of the global star formation history as measured from the Hubble Deep Field. *Astrophys. J. Lett.* **486,** 11–14 (1997).
5. Tresse, L. & Maddox, S. J. The $H\alpha$ luminosity function and star formation rate at $z \sim 0.2$. *Astrophys. J.* **495,** 691–697 (1998).
6. Glazebrook, K., Blake, C., Economou, F., Lilly, S. & Colless, M. Measurement of the star formation rate from $H\alpha$ in field galaxies at $z = 1$. *Mon. Not. R. Astron. Soc.* **306,** 843–856 (1999).
7. Cowie, L., Songaila, A. & Barger, A. J. Evidence for a gradual decline in the universal rest-frame ultraviolet luminosity density for $z < 1$. *Astron. J.* **117,** 2656–2665 (1999).
8. Sullivan, M. *et al.* An ultraviolet-selected galaxy redshift survey—II. The physical nature of star formation in an enlarged sample. *Mon. Not. R. Astron. Soc.* **312,** 442–464 (2000).
9. Scott, S. *et al.* The SCUBA 8-mJy survey: I—Sub-mm maps, sources and source counts. *Mon. Not. R. Astron. Soc.* **331,** 817–838 (2002).
10. Chapman, S. C., Blain, A. W., Ivison, R. J. & Smail, I. R. A median redshift of 2.4 for galaxies bright at submillimetre wavelengths. *Nature* **422,** 695–698 (2003).
11. Ouchi, M. *et al.* A census of Lyman break galaxies at $z = 4$ and 5 in the Subaru Deep Fields: Photometric properties. Preprint at ⟨http://www.arXiv.org/astroph/0309657⟩ (2003).
12. Stanway, E. R., Bunker, A. J. & McMahon, R. G. Lyman break galaxies and the star formation rate of the Universe at $z \sim 6$. *Mon. Not. R. Astron. Soc.* **342,** 439–445 (2003).
13. Shen, S. *et al.* The size distribution of galaxies in the Sloan Digital Sky Survey. *Mon. Not. R. Astron. Soc.* **343,** 978–994 (2003).
14. Jimenez, R., MacDonald, J., Dunlop, J. S., Padoan, P. & Peacock, J. A. Synthetic stellar populations: single stellar populations, stellar interior models and primordial protogalaxies. *Mon. Not. R. Astron. Soc.* **349,** 240–254 (2004).
15. Baldry, I. K. *et al.* The 2dF galaxy redshift survey: Constraints on cosmic star formation history from the cosmic spectrum. *Astrophys. J.* **569,** 582–594 (2002).
16. Glazebrook, K. *et al.* The Sloan Digital Sky Survey: The cosmic spectrum and star formation history. *Astrophys. J.* **587,** 55–70 (2003).
17. Spergel, D. N. *et al.* First year Wilkinson Microwave Anisotropy Probe (WMAP) observations: Determination of cosmological parameters. *Astrophys. J. Suppl.* **148,** 175–194 (2003).
18. Gordon, K. D., Clayton, G. C., Misselt, K. A., Landolt, A. U. & Wolff, M. J. A quantitative comparison of the Small Magellanic Cloud, Large Magellanic Cloud, and Milky Way ultraviolet to near-infrared extinction curves. *Astrophys. J.* **594,** 279–293 (2003).
19. Heavens, A. F., Jimenez, R. & Lahav, O. Massive lossless data compression and multiple parameter estimation from galaxy spectra. *Mon. Not. R. Astron. Soc.* **317,** 965–972 (2000).
20. Reichardt, C., Jimenez, R. & Heavens, A. F. Recovering physical parameters from galaxy spectra using MOPED. *Mon. Not. R. Astron. Soc.* **327,** 849–867 (2001).
21. Panter, B., Heavens, A. F. & Jimenez, R. Star formation and metallicity history of the SDSS galaxy survey: unlocking the fossil record. *Mon. Not. R. Astron. Soc.* **343,** 1145–1154 (2003).
22. Dickinson, M., Papovich, C., Ferguson, H. C. & Budavri, T. The evolution of the global stellar mass density at $0 < z < 3$. *Astrophys. J.* **587,** 25–40 (2003).
23. Dunlop, J. S. in *Deep Millimetre Surveys* (eds Lowenthal, J. D. & Hughes, D. H.) 11–18 (World Scientific, Singapore, 2001).
24. Perez-Gonzalez, P. G. *et al.* Stellar populations in local star-forming galaxies—II. Recent star formation properties and stellar masses. *Mon. Not. R. Astron. Soc.* **338,** 525–543 (2003).
25. Fujita, S. S. *et al.* The $H\alpha$ luminosity function and star formation rate at $z \sim 0.24$ based on Subaru deep imaging data. *Astrophys. J. Lett.* **586,** 115–118 (2003).
26. Waddington, I., Dunlop, J. S., Windhorst, R. A. & Peacock, J. A. The LBDS Hercules sample of milliJansky radio sources at 1.4 GHz: II. Redshift distribution and radio luminosity function. *Mon. Not. R. Astron. Soc.* **328,** 882–896 (2001).
27. Hasinger, G. The X-ray background and AGNs. in *The Restless High Energy Universe* (eds van den Heavel, E. P. J., in't Zand, J. J. M. & Wijers, R. A. M. J.) (Nucl. Phys. B. Suppl. Ser. in the press); preprint at ⟨http://www.arXiv.org/astro-ph/0310804⟩ (2003).
28. Calzetti, D. Reddening and star formation in starburst galaxies. *Astron. J.* **113,** 162–184 (1997).
29. Bruzal, G. & Charlot, S. Spectral evolution of stellar populations using isochrone synthesis. *Astrophys. J.* **405,** 538–553 (1993).

Supplementary Information accompanies the paper on **www.nature.com/nature**.

Acknowledgements We are grateful to M. Pettini and M. Ouchi for helpful remarks. The SDSS is managed by the Astrophysical Research Consortium (ARC) for the Participating Institutions. The participating institutions are The University of Chicago, Fermilab, the Institute for Advanced Study, the Japan Participation Group, The Johns Hopkins University, Los Alamos National Laboratory, the Max Planck Institute for Astronomy (MPIA), the Max Planck Institute for Astrophysics (MPA), New Mexico State University, the University of Pittsburgh, Princeton University, the United States Naval Observatory and the University of Washington.

Competing interests statement The authors declare that they have no competing financial interests.

Correspondence and requests for materials should be sent to A.H. (afh@roe.ac.uk).

Perennial water ice identified in the south polar cap of Mars

Jean-Pierre Bibring[1], Yves Langevin[1], François Poulet[1], Aline Gendrin[1], Brigitte Gondet[1], Michel Berthé[1], Alain Soufflot[1], Pierre Drossart[2], Michel Combes[2], Giancarlo Bellucci[3], Vassili Moroz[4], Nicolas Mangold[5], Bernard Schmitt[6] & the OMEGA team*

[1]*Institut d'Astrophysique Spatiale, Orsay Campus, 91405, France*
[2]*LESIA, Observatoire de Paris/Meudon, 92195 Meudon, France*
[3]*IFSI-INAF, Rome, Italy*
[4]*IKI, Moscow, Russia*
[5]*OrsayTerre, Orsay Campus, 91405, France*
[6]*Laboratoire de Planétologie de Grenoble, 38400, France*

* A list of all the members of the OMEGA team and their affiliations appears at the end of the paper

The inventory of water and carbon dioxide reservoirs on Mars are important clues for understanding the geological, climatic and potentially exobiological evolution of the planet[1]. From the early mapping observation of the permanent ice caps on the martian poles[2,3], the northern cap was believed to be mainly composed of water ice, whereas the southern cap was thought to be constituted of carbon dioxide ice. However, recent missions (NASA missions Mars Global Surveyor and Odyssey) have revealed surface structures[4], altimetry profiles[5], underlying buried hydrogen[6], and temperatures of the south polar regions that are thermodynamically consistent with a mixture of surface water ice and carbon dioxide[7]. Here we present the first direct identification and mapping of both carbon dioxide and water ice in the martian high southern latitudes, at a resolution of 2 km, during the local summer, when the extent of the polar ice is at its minimum. We observe that this south polar cap contains perennial water ice in extended areas: as a small admixture to carbon dioxide in the bright regions; associated with dust, without carbon dioxide, at the edges of this bright cap; and, unexpectedly, in large areas tens of kilometres away from the bright cap.

The ESA/Mars Express Orbiter[8] was inserted into Mars orbit on 25 December 2003. The Observatoire pour la Minéralogie, l'Eau, les Glaces et l'Activité (OMEGA) instrument[9], one of the seven investigating instruments on board, is an imaging spectrometer analysing the diffused solar light and the planetary thermal emission. On each resolved pixel, 1.2 mrad in the instantaneous field of view, OMEGA acquires a spectrum in 352 contiguous spectral channels from 0.35 to 5.1 μm, with a spectral sampling ranging from 7 nm (in the visible) to 13 nm (from 1.0 to 2.7 μm) and 20 nm (from 2.7 to 5.1 μm). A few initial observations were performed soon after Mars orbit insertion, in particular while the spacecraft was overflying the south polar areas. The altitude of observation ranged from ~1,500 km to ~2,000 km, providing an OMEGA surface sampling of ~2 km. OMEGA thus mapped a large fraction of the south polar regions, along four distinct orbits, from 18 January to 11 February 2004 (solar longitude, $L_\odot = 335°$ to 348°)—that is, about one month before the martian southern autumn equinox. At the time of the observations, the Sun's elevation was very low (<10°); however, given the very high performances of OMEGA, several tens of thousands of spectra were acquired with signal-to-noise ratios of >100 over almost the entire spectral domain. From the acquired spectra, it is possible to derive coupled maps of a variety of parameters and properties: in particular, the major icy constituents, CO_2 and H_2O, have several unambiguous diagnostic spectral signatures enabling the mapping of their respective distributions over the imaged areas (see below).

The OMEGA spectral images exhibit well-characterized high albedo perennial polar ice patterns. From their near-infrared spectrum, we can assert that these bright areas are those where